merical calculation of the reflection efficiency on a grating, based on Rigorous Coupled-Wave Analysis (RCWA)[9]. A grating with a rectangular profile with pitch of 15μm in duty cycle 50%, the dielectric function of polycrystalline gold for a grating material, and incident light as a plane wave propagating in vacuum at wavelength of 10.6μm, are assumed. Fig. 1(C) shows clear dips on the reflection efficiency at where the grating depth is roughly from 0.2 to 1.3μm, due to energy conversion from propagating light to SPPs, indicating SPP excitation on the grating. We expected the effective coupling efficiency takes the maximum value around the depth 0.8μm in this experiment, taking the certain angular divergence of incident light into consideration. The height of the grating structure was designed to be 0.8μm, in a reasonable agreement with a previous report estimating optimum grating depth for a rectangular grating to be 10%-15% of the wavelength in mid-infrared range[8].

The sets of gold gratings and a waveguide were fabricated on a gold base layer on a glass substrate, by using electron beam lithography, thermal evaporation, and lift-off process. The gold base with thickness 200nm was thermally evaporated on a glass substrate with a Chromium adhesion layer with thickness 5nm, after cleaning the substrate with acetone and ethanol. Then, EB resist (OEBR-CAP112PM, TOK) was spin-coated on the base with thickness 1700nm to be exposed in electron beam for development. Finally, gold with thickness 800nm was evaporated on the top of the developed resist, and the resist was lifted off using acetone. The whole fabrication process was conducted at room temperature. During the evaporation, we maintained the evaporation rate of gold to be 0.4nm/s, and the pressure inside the vacuum chamber less than 3×10^{-5}Torr.

4 Suface Characterization

Isotropic deposition of gold and flat surface were confirmed. The surface state changes drastically after annealing as shown in Fig. 2. Surface roughness is estimated as 3.58nm for the as-grown sample, 16.2nm for the sample annealed at 600°C, and 18.3nm for the sample annealed twice at 600°C and 700°C, by calculating two-dimensional root mean squares of deviations in height data. As annealing applied, the surface roughness increased. The gratings were not significantly transformed after the annealing. However, there appear to be pinholes on the surface of waveguide with 1μm order as the annealing applied.

For detailed characterization of the surface morphology, we identified crystal grains on the surface based on watershed algorithm[10], to estimate diameter of the crystal grains in the assumption that a grain is close to spherical shape. Average grain diameter corresponds 70nm, 190nm, and 180nm, respectively for the as-grown sample, the sample annealed at 600°C, and the sample annealed twice at 600°C and 700°C. The grain size has significantly increased as the first annealing at 600°C was applied, whereas there does not seem to be grain enlargement by the second annealing at 700°C, relying on the AFM measurement.

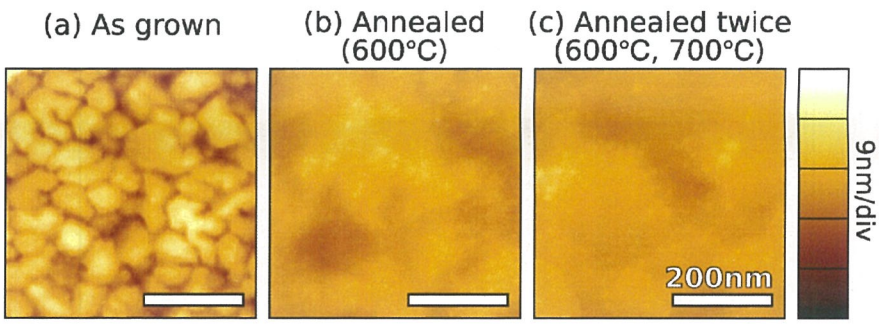

Figure 2: Height plots on the surface of waveguides based on AFM. Crystal grain diameter is estimated to be 70nm for the as-grown sample (a), 190nm for the sample annealed at 600°C (b), and 180nm for the sample annealed twice at 600°C and 700°C (c).

5 Result

Fig. 3 shows the power out-coupled from the propagating SPPs along the waveguides with a different length L, measured for each of the sample before and after annealing. Each of the out-coupled power is normalized for ignoring systematic errors, originated from a laser-power drift and a minor shift of SPP-light coupling efficiency on the gratings by the annealing. By the method of least squares, they